



The Tarda Meteorite: A Window into the Formation of D-type Asteroids

Yves Marrocchi¹, Guillaume Avice², and Jean-Alix Barrat³¹ Université de Lorraine, CNRS, CRPG, UMR 7358, Vandœuvre-lès-Nancy, F-54501, France; yvesm@crpg.cnrs-nancy.fr² Université de Paris, Institut de physique du globe de Paris, CNRS, F-75005 Paris, France³ Université de Brest, CNRS, IRD, Ifremer, LEMAR, F-29280 Plouzané, France

Received 2021 April 7; revised 2021 April 18; accepted 2021 April 19; published 2021 May 19

Abstract

Dynamic models of solar system evolution suggest that D-type asteroids formed beyond Saturn's orbit and represent invaluable witnesses of the prevailing conditions in the outer solar system. Here, we report a comprehensive petrographic and isotopic characterization of the carbonaceous chondrite Tarda, a recent fall recovered in the Moroccan Sahara. We show that Tarda shares strong similarities with the D-type-derived chondrite Tagish Lake, implying that Tarda represents a rare sample of D-type asteroids. Both Tarda and Tagish Lake are characterized by the presence of rare ¹⁶O-rich chondrules and chondrule fragments, high C/H ratios, and enrichments in deuterium, ¹⁵N, and ¹³C. By combining our results with literature data on carbonaceous chondrites related to C-type asteroids, we show that the outer solar system 4.56 Gy ago was characterized by large-scale oxygen isotopic homogeneities in (i) the water–ice grains accreted by asteroids and (ii) the gas controlling the formation of FeO-poor chondrules. Conversely, the zone in which D-type asteroids accreted was significantly enriched in deuterium relative to the formation regions of C-type asteroids, features likely inherited from unprocessed, D-rich, molecular-cloud materials.

Unified Astronomy Thesaurus concepts: Asteroids (72); Isotopic abundances (867); Trans-Neptunian objects (1705); Carbonaceous chondrites (200)

1. Introduction

Asteroids are small bodies orbiting the Sun that result from the complex evolution of planetesimals that formed early during the history of the protoplanetary disk (Delbo et al. 2017). Most known asteroids are presently located in the main asteroid belt, between the orbits of Mars and Jupiter (heliocentric distances of ~ 2 – 3.2 au; DeMeo & Carry 2014). Asteroids are characterized by spectroscopically distinct features that, in general, correspond to distinct mineralogical and chemical compositions (DeMeo & Carry 2014). D-type asteroids are dark bodies whose mineral compositions are poorly known due to the low reflection intensities of their surfaces (Gartrelle et al. 2021). Nonetheless, spectral features indicate the presence of water ice, organics, phyllosilicates, and anhydrous minerals (e.g., Mg-rich olivine; Barucci et al. 2018; Gartrelle et al. 2021). Although rare in the main asteroid belt ($\sim 2\%$; DeMeo & Carry 2014), D-type asteroids are the most abundant (i) at the outer edge of the main belt (i.e., ~ 3.0 – 3.2 au) and (ii) among Jupiter Trojans (i.e., 5.2 au; 66%–84% of all Trojans). D-type asteroids could have formed beyond the orbit of Neptune and potentially as far as the Kuiper Belt (i.e., 30–50 au; Levison et al. 2009; Vokrouhlický et al. 2016). Numerical simulations suggest that the dynamic evolution of the giant planets' orbits led to the capture of D-type asteroids from a primordial trans-Neptunian disk (Morbidelli et al. 2005) and their subsequent implantation into the outer main asteroid belt and at the Jupiter Trojan orbit (Levison et al. 2009; Vokrouhlický et al. 2016). D-type asteroids thus represent invaluable witnesses of the conditions that prevailed in the outer circumsolar disk 4.56 Ga.

Chondrites are leftover solids from the evolution of the circumsolar disk. Their diversity attests to the different asteroid populations currently observed in the solar system. For instance, carbonaceous chondrites are genetically linked to water-rich C-type asteroids, whereas ordinary chondrites are

related to dry S-type asteroids. Samples of D-type asteroids have not been unequivocally confirmed, with the possible exception of three specific meteorites: WIS 91600 (Hiroi et al. 2005), MET 00432 (Nakamura et al. 2013), and Tagish Lake (Brown et al. 2000). Among them, the Tagish Lake chondrite has been studied in detail because a significant amount (~ 10 kg) of it was quickly recovered after its fall (Hiroi 2001). Although Tagish Lake might not be representative of the surface compositions of D-type asteroids, as previously suggested by Izawa et al. (2015), it may represent the aqueously altered cores of these peculiar bodies (Vernazza et al. 2017). A genetic link between Tagish Lake and D-type asteroids has also been proposed based on (i) its weak magnetic paleointensity (Byrson et al. 2020; Weiss et al. 2021) and (ii) the systematic presence of ¹³C-rich carbonates (Fujiya et al. 2019). In addition, Tagish Lake is characterized by high abundances of carbon and presolar grains, and large deuterium and ¹⁵N enrichments (Nakamura-Messenger et al. 2006), implying its formation in a cold region of the disk (Brown et al. 2000). Despite the fundamental importance of Tagish Lake, our knowledge of the characteristics of the outer solar system at the time of its formation is limited by the rarity of samples derived from D-type asteroids in meteorite collections.

The Tarda chondrite fell in the Moroccan Sahara on 2020 August 25, and the first pieces of it were collected the following day. Around 4 kg were ultimately recovered, and initial petrographic and geochemical analyses suggest that Tarda corresponds to a type-2 ungrouped carbonaceous chondrite (Chennaoui Aoudjehane et al. 2021). More specifically, Tarda is characterized by a bulk oxygen isotopic composition (i) lying between those of CI and CY chondrites (Clayton & Mayeda 1984; King et al. 2019; Chennaoui Aoudjehane et al. 2021) and (ii) similar to that estimated for Tagish Lake (Brown et al. 2000). Here, we report a comprehensive description of the Tarda chondrite. Our results

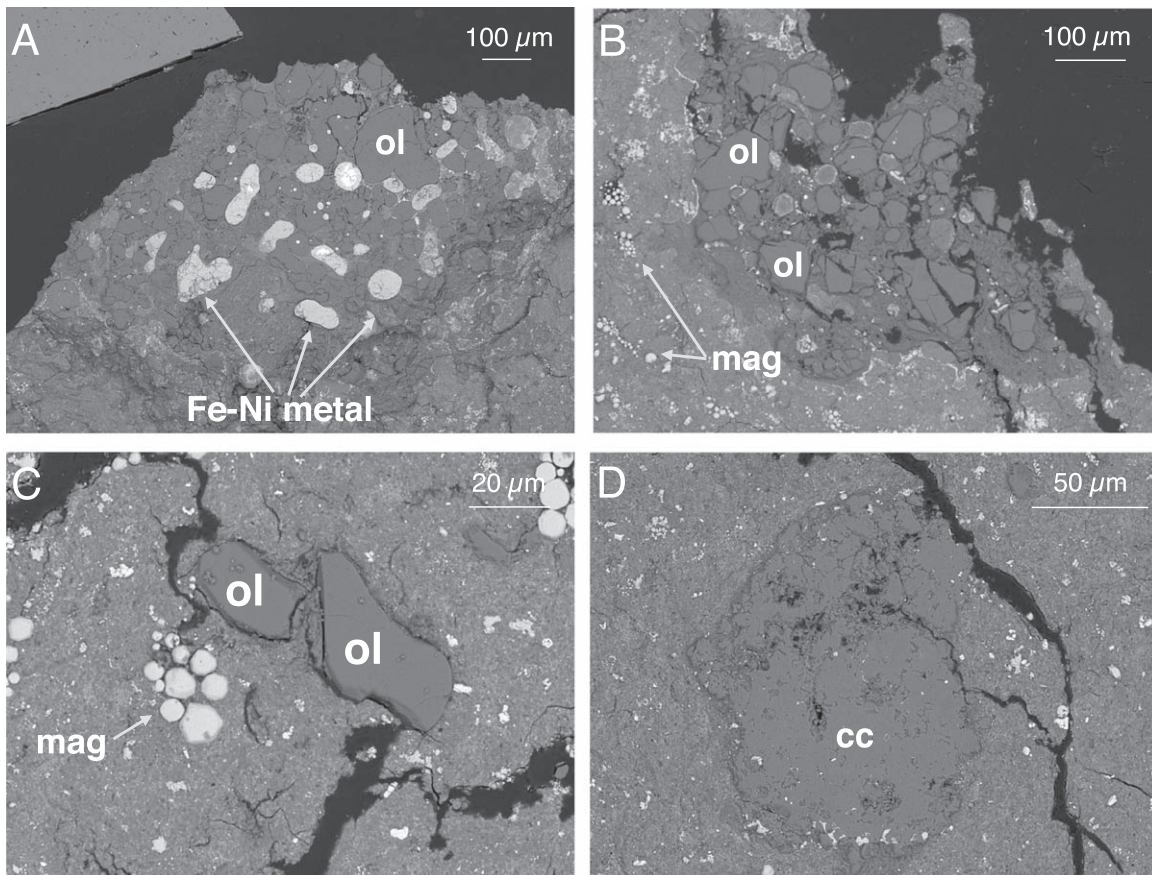


Figure 1. Back-scattered electron images of (A, B) porphyritic, FeO-poor chondrules and isolated (C) olivine (ol) and (D) dolomite (cc) grains in the Tarda carbonaceous chondrite. Framboidal magnetite (mag) grains are also visible in (C).

demonstrate that Tarda shares numerous similarities with Tagish Lake and thus corresponds to a D-type asteroid formed in the outer part of the solar system. We use our data to discuss the peculiar characteristics of bodies formed beyond the orbit of Saturn 4.56 Ga ago.

2. Material and Methods

We characterized the Tarda carbonaceous chondrite based on (i) petrographic observations (scanning electron microscope and electron microprobe), (ii) bulk mineralogical and chemical analyses (X-ray diffraction (XRD) and inductively coupled plasma-sector field mass spectrometry), and (iii) both in situ (i.e., phase-specific, secondary ion mass spectrometry) and bulk isotopic measurements (elemental analyzer/isotope ratio mass spectrometry). All analytical techniques are reported in the supplementary information. Isotopic compositions are reported as per-mil variations relative to that of a standard using delta notation as $\delta^{XE} = ((^{XE}/^{YE})_{\text{sample}} / (^{XE}/^{YE})_{\text{standard}}) - 1 \times 1000$, where E indicates the element, and X and Y are the mass numbers of the heavy and light isotopes, respectively.

3. Results

Our observations of Tarda revealed an abundant fine-grained matrix containing porphyritic chondrules and isolated olivine grains (hereafter, IOGs; Figure 1). All observed olivines are forsterites with Mg# ($=\text{Mg}/[\text{Mg} + \text{Fe}] \times 100$) ranging from 98.7 to 99.3 (Table 2). No calcium–aluminum–rich inclusions (CAIs) or amoeboid olivine aggregates were observed in the

two surveyed sections. Magnetite was frequently observed as framboidal clusters in the fine-grained matrix (Figure 1(C)). A few carbonates (dolomite) were also observed (Figure 1(D)). Crystalline phases identified in diffraction patterns were magnetite, dolomite, Fe-sulfides, and olivine (Figure 2). We attribute the broad diffraction peaks observed at 19° and 60° (2θ Cu $K\alpha_1$; Figure 2) to the presence of fine-grained phyllosilicates (King et al. 2019).

Bulk chemical compositions obtained for two aliquots of Tarda showed drastically different results (Figure 5; Table 3). The first aliquot was enriched in rare earth elements (REEs) relative to CI chondrites (Figure 5(A); Barrat et al. 2012), with a flat REE pattern, and had a bulk composition enriched in refractory elements and depleted in volatile elements (Figure 5(B)), similar to that of Tagish Lake (Friedrich et al. 2002; Pourmand et al. 2012). The second aliquot showed an extreme enrichment in ultra-refractory elements that could result from either (i) a higher abundance of refractory inclusions than in the first aliquot or (ii) contamination during crushing; therefore, we only consider the first aliquot in the following discussion.

The two analyzed aliquots of Tarda contained 8.54 and 8.57 wt.% H_2O , equivalent to 0.948 and 0.952 wt.% H, respectively, and had respective H isotopic values of $\delta\text{D} = 678.4\text{‰}$ and 681.6‰ (Figure 3, Table 1). Three other aliquots were separated for analyses of C and N abundances and isotopic compositions; these aliquots contained 4.06 wt.% C and 0.29 wt.% N and had isotopic compositions of $\delta^{13}\text{C} = 10.9\text{‰}$ and $\delta^{15}\text{N} = 55.3\text{‰}$, respectively (Table 1).

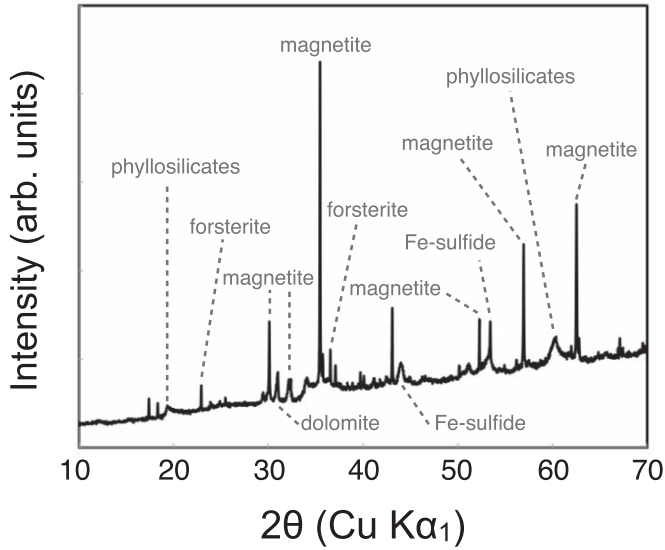


Figure 2. Position-sensitive X-ray diffraction pattern of the Tarda carbonaceous chondrite. The presence of phyllosilicates at 19 and 60° 2θ suggests that Tarda did not experience dehydration during the evolution of its parent body.

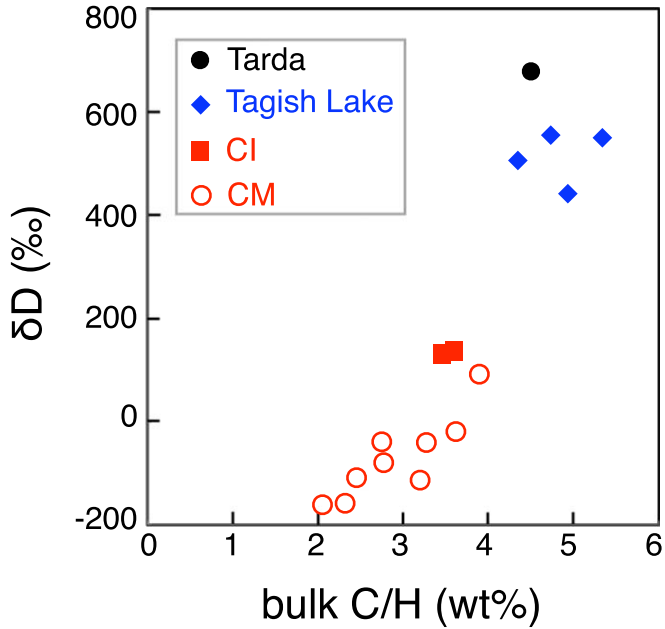


Figure 3. Comparison of the bulk D/H (as δD) vs. C/H ratios of Tarda and Tagish Lake, as well as those of CM and CI chondrites (data measured after pre-degassing of the samples; Vacher et al. 2016, 2020).

Table 1

Bulk Hydrogen, Carbon, and Nitrogen Abundances and Isotopic Compositions of Tarda

	H (wt%)	δD ‰	C (wt%)	$\delta^{13}C$ ‰	N (wt%)	$\delta^{15}N$ ‰
Tarda 1	0.948	678.4				
Tarda 2	0.952	681.6				
Tarda 3			4.00	11.3	0.28	54.7
Tarda 4			4.06	10.7	0.28	55.3
Tarda 5			4.11	10.7	0.30	55.9

The oxygen isotopic compositions of Mg-rich chondrules and IOGs define a linear correlation (Figure 4(A), $\delta^{17}O = [0.991 \pm 0.142] \times \delta^{18}O - [2.8 \pm 0.8]$, $r^2 = 0.98$) and plot along the

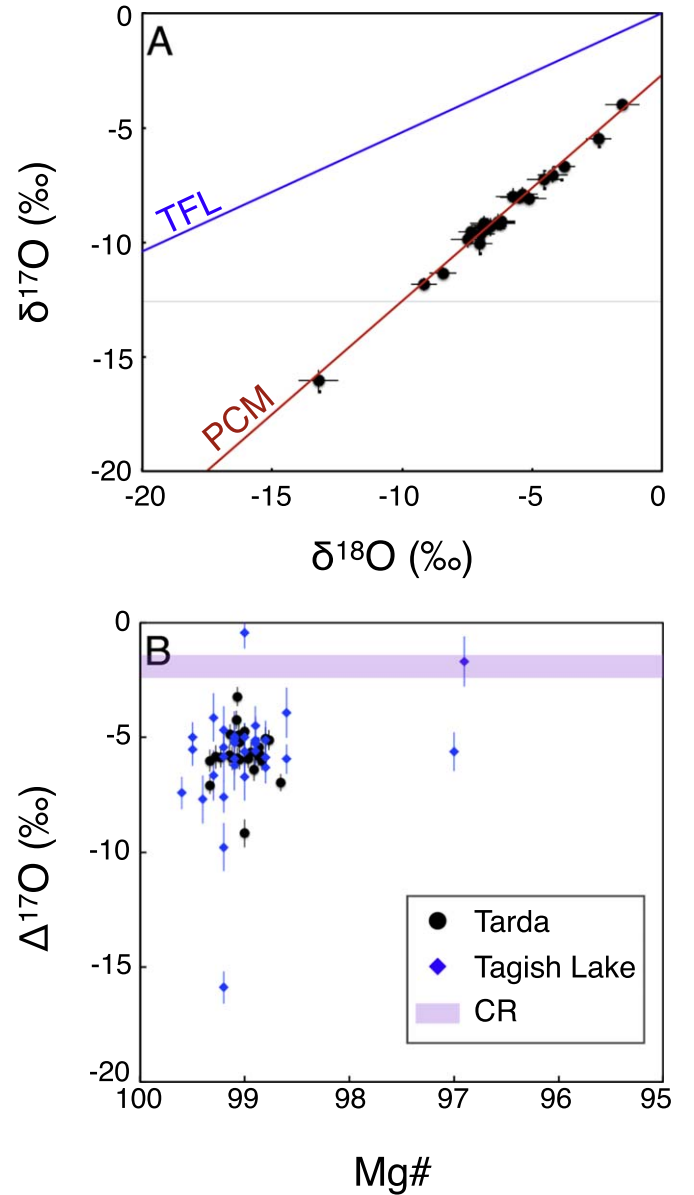


Figure 4. (A) Oxygen isotopic compositions and (B) oxygen isotopic fractionations of chondrule olivines and isolated olivine grains in Tarda and Tagish Lake (Ushikubo & Kimura 2021). The range of oxygen isotopic compositions of host olivine grains in CR chondrules is also shown (purple rectangle). The primitive chondrule mineral line (PCM) and terrestrial fractionation line (TFL) are shown for reference.

primitive chondrule minerals line (Ushikubo et al. 2012), with $\delta^{18}O$ and $\delta^{17}O$ ranging from -13.2‰ to -1.5‰ and from -16.1‰ to -4.0‰ , respectively (Figure 4(A), Table 2).

Excluding chondrule Ch-1, all other individual chondrules and IOGs are characterized by limited O isotopic variabilities but show average $\delta^{18}O$ and $\delta^{17}O$ values ranging from -7.1‰ to -2.6‰ and from -9.8‰ to -5.4‰ , respectively (Table 2). The O isotopic fractionations of chondrule olivines and IOGs, expressed as $\Delta^{17}O = \delta^{17}O - 0.52 \times \delta^{18}O$, range from -9.2‰ to -3.2‰ , but most have $\Delta^{17}O$ values between -5‰ and -6‰ (Figure 4(B); Table 1). Concentrations of Al_2O_3 , TiO_2 , CaO , MnO , and NiO range from 0.04–0.23 wt.%, 0.05–0.09 wt.%, 0.11–0.41 wt.%, 0.07–0.31 wt.%, and 0.008–0.010 wt.%, respectively (Table 1).

Table 2
Oxygen Isotopic Compositions and Chemical Compositions of Chondrule and Isolated Olivine Grains in Tarda

Chondrule	$\delta^{18}\text{O}$	2σ	$\delta^{17}\text{O}$	2σ	$\Delta^{17}\text{O}$	2σ	SiO ₂	FeO	Al ₂ O ₃	CaO	MnO	MgO	Cr ₂ O ₃	TiO ₂	NiO	Total	Fo#
detection limit							0.03	0.07	0.03	0.03	0.04	0.03	0.07	0.04	0.07		
Ch-1	-5.11	0.67	-8.10	0.30	-5.44	0.46	42.47	1.14	0.04	0.19	0.14	55.75	0.50	bdl	bdl	100.2	98.9
	-4.21	0.59	-7.06	0.34	-4.87	0.46	42.06	0.87	0.04	0.22	0.11	56.40	0.46	0.06	bdl	100.2	99.1
	-5.48	0.73	-8.04	0.28	-5.19	0.47	42.31	0.96	0.08	0.24	0.17	56.22	0.34	bdl	0.08	100.4	99.1
	-6.23	0.59	-9.17	0.26	-5.93	0.40	42.57	1.04	0.09	0.31	0.22	55.86	0.45	bdl	bdl	100.5	99.0
	-5.37	0.60	-7.90	0.30	-5.11	0.44	42.30	1.24	0.11	0.24	0.23	55.87	0.52	0.07	bdl	100.6	98.8
	-13.22	0.78	-16.04	0.47	-9.17	0.62	42.19	1.01	0.04	0.11	0.18	56.00	0.53	0.05	bdl	100.1	99.0
Ch-2	-6.59	0.62	-9.33	0.40	-5.90	0.52	42.36	0.89	0.13	0.14	0.12	56.34	0.21	0.07	bdl	100.3	99.1
	-4.53	0.66	-7.26	0.39	-4.90	0.52	42.48	0.95	0.11	0.26	0.15	55.78	0.39	bdl	bdl	100.1	99.1
	-5.73	0.67	-8.01	0.37	-5.04	0.51	42.39	1.21	0.13	0.37	0.11	56.04	0.45	bdl	bdl	100.7	98.8
	-6.21	0.58	-9.18	0.31	-5.95	0.43	42.31	0.96	0.21	0.18	0.07	56.17	0.57	0.09	bdl	100.6	99.1
	-6.70	0.65	-9.25	0.32	-5.77	0.46	42.15	0.86	0.05	0.25	0.26	56.07	0.42	bdl	bdl	100.1	99.1
Ch-3	-7.47	0.67	-9.90	0.35	-6.01	0.49	42.51	0.67	0.04	0.27	0.14	56.12	0.26	bdl	bdl	100.0	99.3
	-6.20	0.57	-9.08	0.33	-5.86	0.45	42.36	0.77	0.06	0.16	0.09	55.72	0.40	bdl	bdl	99.6	99.2
	-7.02	0.50	-10.06	0.40	-6.41	0.48	42.48	1.11	0.12	0.21	0.19	56.49	0.39	bdl	0.10	101.1	98.9
	-7.34	0.49	-9.57	0.27	-5.75	0.37	42.67	1.14	0.04	0.38	0.14	55.34	0.17	bdl	bdl	99.9	98.9
	-8.43	0.51	-11.35	0.26	-6.96	0.37	42.38	1.36	0.04	0.41	0.10	56.04	0.48	bdl	bdl	100.8	98.7
	-6.74	0.71	-9.41	0.28	-5.90	0.46	42.22	0.94	0.07	0.16	0.21	56.11	0.51	bdl	bdl	100.2	99.1
	-6.31	0.65	-9.13	0.38	-5.85	0.51	42.36	0.73	0.06	0.24	0.20	56.30	0.42	0.06	bdl	100.4	99.3
IOG-1	-9.16	0.49	-11.85	0.28	-7.09	0.38	42.20	0.67	0.11	0.27	0.14	55.88	0.39	bdl	bdl	99.7	99.3
IOG-2	-6.86	0.53	-9.37	0.33	-5.80	0.43	42.33	1.14	0.13	0.22	0.31	55.97	0.62	bdl	bdl	100.7	98.9
	-6.85	0.52	-9.20	0.37	-5.64	0.46	42.55	1.07	0.08	0.22	0.28	56.07	0.28	bdl	bdl	100.6	98.9
	-6.95	0.51	-9.64	0.29	-6.03	0.39	42.41	1.18	0.09	0.38	0.14	56.23	0.37	bdl	bdl	100.8	98.8
IOG-3	-1.53	0.67	-4.01	0.25	-3.22	0.42	42.74	0.94	0.11	0.31	0.08	56.03	0.39	bdl	bdl	100.6	99.1
	-2.43	0.49	-5.50	0.33	-4.24	0.41	42.39	0.93	0.16	0.28	0.16	56.24	0.42	0.08	bdl	100.7	99.1
	-3.77	0.43	-6.69	0.25	-4.73	0.34	42.47	1.01	0.23	0.17	0.17	56.08	0.35	bdl	bdl	100.5	99.0

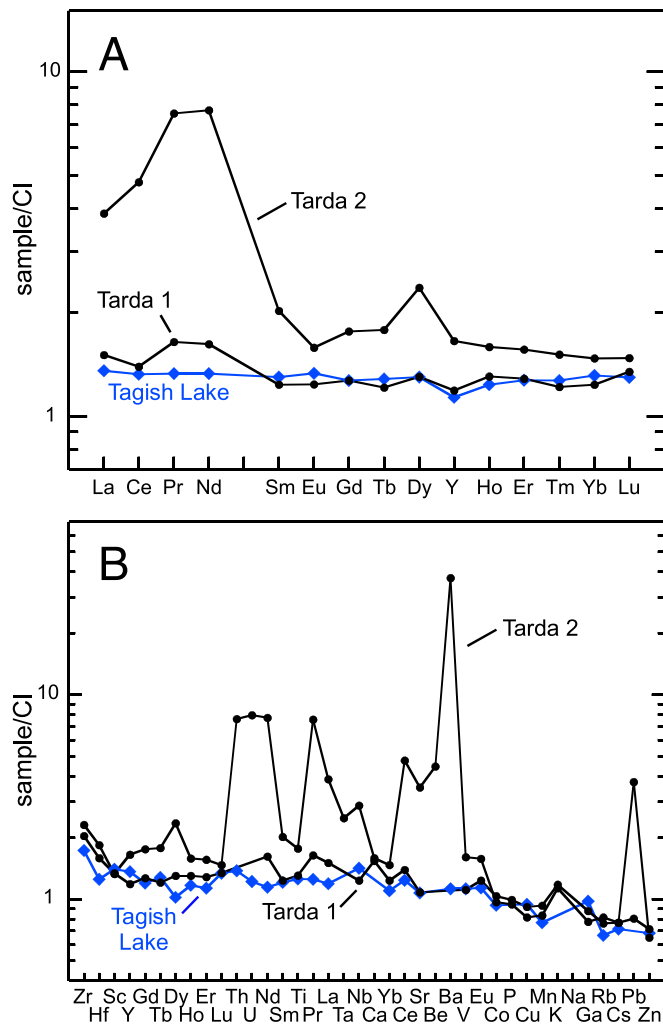


Figure 5. (A) REE and (B) bulk trace element patterns of Tarda and Tagish Lake (Pourmand et al. 2012) normalized to the average composition of Orgueil (Barrat et al. 2012).

4. Discussion

4.1. Tarda's Genetic Relationship with Other Known Chondrite Types

Among chondrites, the Tarda meteorite shows peculiar characteristics that led to its classification as C2 ungrouped. The bulk oxygen isotopic compositions of fragments of Tarda plot below the terrestrial fractionation line and show a bimodal distribution characterized by $\delta^{17}\text{O}$ values near those of either CI or CY chondrites (King et al. 2019; Chennaoui Aoudjehane et al. 2021). In addition, the ^{54}Cr isotopic composition of Tarda is close to that estimated for CR chondrites (Dey et al. 2021). However, our results demonstrate that Tarda has no genetic link with CI, CY, or CR chondrites for six reasons. First, chondrules and IOGs are rare but not uncommon in Tarda (Figure 1; Jacquet et al. 2021), whereas no (pseudomorphosed)-chondrule has yet been reported in CI chondrites (Piralla et al. 2020). Second, compared to CI chondrites, the bulk chemical composition of Tarda is significantly enriched in REEs and refractory elements and depleted in volatile elements (Figure 5, Table 3). Third, the diffraction pattern of Tarda reveals phyllosilicates (Figure 2) that comprise around 72% of the bulk (King et al. 2021), implying that Tarda did not experience dehydration as did CY chondrites (King et al. 2019). Fourth, the hydrogen

Table 3

REE and Bulk Trace Element Patterns of Tarda Normalized to the Average Composition of Orgueil

lab.		Tarda 1 CRPG	Tarda 2 IUEM
SiO ₂	wt%	27.09	
TiO ₂	wt%	0.098	0.133
Al ₂ O ₃	wt%	2.084	
FeO	wt%	26.34	
MnO	wt%	0.228	0.206
MgO	wt%	18.89	
CaO	wt%	1.81	1.87
Na ₂ O	wt%	0.60	
K ₂ O	wt%	0.08	0.075
P ₂ O ₅	wt%	0.23	0.219
L.O.I.	wt%	17.5	
Be	$\mu\text{g g}^{-1}$	n.d.	0.101
Sc	$\mu\text{g g}^{-1}$	7.84	7.79
V	$\mu\text{g g}^{-1}$	58.25	84.40
Cr	$\mu\text{g g}^{-1}$	3283	n.d.
Co	$\mu\text{g g}^{-1}$	539	504
Ni	$\mu\text{g g}^{-1}$	11648	n.d.
Cu	$\mu\text{g g}^{-1}$	117	104
Zn	$\mu\text{g g}^{-1}$	217	197
Ga	$\mu\text{g g}^{-1}$	8.31	7.37
Ge	$\mu\text{g g}^{-1}$	25.91	n.d.
As	$\mu\text{g g}^{-1}$	3.90	n.d.
Rb	$\mu\text{g g}^{-1}$	1.78	1.91
Sr	$\mu\text{g g}^{-1}$	8.38	27.28
Y	$\mu\text{g g}^{-1}$	1.86	2.58
Zr	$\mu\text{g g}^{-1}$	7.2	8.14
Nb	$\mu\text{g g}^{-1}$	0.357	0.831
Mo	$\mu\text{g g}^{-1}$	1.89	n.d.
Sb	$\mu\text{g g}^{-1}$	0.37	n.d.
Sn	$\mu\text{g g}^{-1}$	1.17	n.d.
Cs	$\mu\text{g g}^{-1}$	0.145	0.145
Ba	$\mu\text{g g}^{-1}$	n.d.	91.64
La	$\mu\text{g g}^{-1}$	0.3541	0.910
Ce	$\mu\text{g g}^{-1}$	0.8362	2.87
Pr	$\mu\text{g g}^{-1}$	0.1494	0.687
Nd	$\mu\text{g g}^{-1}$	0.7512	3.58
Sm	$\mu\text{g g}^{-1}$	0.1888	0.309
Eu	$\mu\text{g g}^{-1}$	0.0725	0.0927
Gd	$\mu\text{g g}^{-1}$	0.2614	0.363
Tb	$\mu\text{g g}^{-1}$	0.0454	0.0669
Dy	$\mu\text{g g}^{-1}$	0.3305	0.600
Ho	$\mu\text{g g}^{-1}$	0.0738	0.0898
Er	$\mu\text{g g}^{-1}$	0.2135	0.259
Tm	$\mu\text{g g}^{-1}$	0.0319	0.0395
Yb	$\mu\text{g g}^{-1}$	0.2075	0.248
Lu	$\mu\text{g g}^{-1}$	0.0331	0.0363
Hf	$\mu\text{g g}^{-1}$	0.171	0.197
Ta	$\mu\text{g g}^{-1}$	0.0245	0.0369
W	$\mu\text{g g}^{-1}$	n.d.	0.52
Pb	$\mu\text{g g}^{-1}$	2.16	10.03
Bi	$\mu\text{g g}^{-1}$	0.09	n.d.
Th	$\mu\text{g g}^{-1}$	0.0581	0.215
U	$\mu\text{g g}^{-1}$	n.d.	0.0613

Note. They have been measured in two different laboratories (CRPG and IUEM).

isotopic composition of Tarda ($\delta\text{D} = +680\text{‰}$; Figure 3) is D-rich compared to those reported for CI and CY chondrites, $+135\text{‰}$ and -106‰ , respectively (Figure 3; Vacher et al. 2020). Fifth, Tarda is strongly enriched in ^{13}C ($\delta^{13}\text{C} = +10.9\text{‰}$)

compared to CI and CY chondrites ($\delta^{13}\text{C} = -11.8\%$ and -12.9% , respectively; Alexander et al. 2012; Vacher et al. 2020). Finally, the $\delta^{17}\text{O}$ values of chondrule olivines and IOGs are around -6% (Figure 4(B)), significantly different from those reported for CR anhydrous silicates (i.e., $\delta^{17}\text{O} \approx -2\%$; Tenner et al. 2018). These features demonstrate that Tarda is not related to CR, CI, or CY chondrites, but instead represents a specific type of carbonaceous chondrite with bulk $\delta^{17}\text{O}$ values plotting near the TFL.

Interestingly, the bulk oxygen isotopic composition of Tagish Lake ($\delta^{17}\text{O} = -0.83 \pm 0.26\%$; Brown et al. 2000) is relatively close to that of Tarda ($-0.13 \pm 0.15\%$; Chennaoui Aoudjehane et al. 2021), suggesting a potential link with this peculiar chondrite. Indeed, several observations corroborate this hypothesis. Chondrule olivines and IOGs in Tarda show $\delta^{17}\text{O}$ values similar to those reported for olivines in Tagish Lake, with values around -6% (Figure 4(B); Ushikubo & Kimura 2021). In addition, both chondrites are characterized by large D-enrichments; $\delta\text{D} = +680\%$ in Tarda and $+442.3$ to $+556.36\%$ in Tagish Lake (Alexander et al. 2012; Vacher et al. 2020). Furthermore, Tarda and Tagish Lake plot in the same field in the δD versus C/H diagram (Figure 3, Table 1) and have similar, isotopically heavy bulk $\delta^{13}\text{C}$ ($+10.9\%$ and $+4.7\%$, respectively; Vacher et al. 2020) and $\delta^{15}\text{N}$ compositions ($+55.3\%$ and $+66.2\%$, respectively; Alexander et al. 2012). Finally, the bulk chemical composition and REE pattern of Tarda are similar to those determined for Tagish Lake (Friedrich et al. 2002; Pourmand et al. 2012, Figure 5; Table 3). Our data therefore demonstrate that Tarda is genetically related to Tagish Lake and thus represents a new sample of D-type asteroids.

4.2. Implications for the Isotopic Characteristics of the D-type Asteroid Accretion Region

The peculiar characteristics of both Tarda and Tagish Lake provide a window into the characteristics of the region in which D-type asteroids accreted and the isotopic structure of the outer solar system. We now discuss our results in light of previous results on Tagish Lake.

The low abundances of chondrules and IOGs in both Tagish Lake and Tarda could result from intensive fluid circulation processes, as observed in some CM1 chondrites. However, the limited volatile-depletion observed in Tarda suggests that chondrules were never a significant constituent of Tarda (Figure 5(B)). Conversely, such a low degree of volatile-depletion could be interpreted as the result of (i) ineffective anhydrous silicate formation in the D-type asteroid accretion region or (ii) limited large-scale transport from other regions of the disk. Interestingly, the $\Delta^{17}\text{O}$ values of chondrule olivines in Tarda and Tagish Lake (i.e., $\sim -6\%$) are similar to the large majority of FeO-poor chondrules and IOGs reported in other carbonaceous chondrites, with the exception of CR chondrites (i.e., $\Delta^{17}\text{O} \approx -2\%$; see Tenner et al. 2018 for a compilation). Assuming transport between reservoirs in the disk, this would suggest that chondrules in the D-type asteroid-forming region originated from a C-type reservoir. Alternatively, local chondrule formation would imply large-scale oxygen isotopic homogeneity because chondrule olivines formed via interactions between (partially) molten chondrule precursors and the ambient gas (e.g., Marrocchi et al. 2018, 2019; Tenner et al. 2018; Ushikubo & Kimura 2021).

Interestingly, the peculiar ^{26}Al and ^{54}Cr isotopic signatures of CR chondrules have been interpreted as resulting from (i) the incorporation of ^{26}Al -poor primordial materials inherited from the molecular cloud and (ii) their formation beyond the orbits of the giant planets (van Kooten et al. 2016). These authors suggested a similar outer solar system origin for the ^{16}O - and ^{26}Al -poor chondrules and chondrule fragments sampled from the Jupiter-family comet Wild 2 by the Stardust mission, which are generally interpreted as having formed late in the inner circumsolar disk and radially transported to the cometary accretion region (Ogliore et al. 2012). Consequently, they proposed that chondrule formation was not limited to the innermost part of the solar system, but instead occurred throughout the disk, including the region in which D-type asteroids accreted. If correct, this implies that the O isotopic composition of the gas that interacted with FeO-poor chondrules was homogeneous at the scale of the C- and D-type asteroid accretion regions.

Both Tarda and Tagish Lake are dominated by phyllosilicates (Brown et al. 2000; King et al. 2021), implying that D-type asteroids accreted water-ice grains with Earth-like O isotope compositions (i.e., $\delta^{17}\text{O} \approx 0\%$). Indeed, the water released during the pyrolysis of Tagish Lake had a terrestrial oxygen isotopic composition (Baker et al. 2002). Similar to CI chondrites (Piralla et al. 2020), neither Tarda nor Tagish Lake show any evidence of $^{17,18}\text{O}$ -rich water formed via the self-shielding of ^{16}O -rich nebular $\text{CO}_{(\text{g})}$ by UV light in the molecular cloud or outer solar system (e.g., Krot et al. 2020). This implies that, at the time when chondritic parent bodies formed, the outer solar system was characterized by oxygen isotopic compositions similar to those of the terrestrial planets such as Earth and Mars. However, these peculiar isotopic characteristics do not preclude the occurrence of self-shielding processes because carbonaceous chondrites accreted relatively late during the disk's evolution (i.e., ≥ 2.5 Myr after the formation of CAIs; Sugiura & Fujiya 2014). Hence, $^{17,18}\text{O}$ -rich water-ice grains could have experienced rapid thermal processing and O isotopic reequilibration with amorphous silicates—the main constituent of chondritic matrices (Le Guillou et al. 2015)—as recently experimentally demonstrated (Yamamoto et al. 2018). This would have shifted the O isotopic composition of water toward terrestrial values, as inferred from the $\delta^{17}\text{O}$ values of aqueously formed minerals in other carbonaceous chondrites (e.g., Doyle et al. 2015). Nevertheless, the bulk O isotopic compositions of Tarda, Tagish Lake, and other carbonaceous chondrites indicate that water in the outer solar system (beyond several tens of astronomical units) had homogenous, Earth-like, oxygen isotopic compositions.

Another peculiar feature of Tarda is its strong enrichment in D (Figure 3; Vacher et al. 2020), which is consistent with the D-rich bulk and in situ compositions of Tagish Lake (Nakamura-Messenger et al. 2006; Patzek et al. 2020; Vacher et al. 2020). D-rich signatures of chondrites are generally interpreted as resulting from either (i) the accretion of D-rich organics and/or water-ice grains (Vacher et al. 2020) or (ii) the aqueous oxidation of Fe-Ni metal beads followed by H_2 -loss and Rayleigh-type isotopic fractionation (Sutton et al. 2017). The latter process is, however, ineffective for enriching water-rich chondrites such as Tarda in deuterium as their D/H ratios could not be buffered due to their large amount of initial water (Vacher et al. 2020). In addition, this is inconsistent with the higher H concentration and isotopic composition of Tarda

relative to Tagish Lake (Figure 3), as the opposite isotopic characteristics would be expected (Vacher et al. 2021). Our data thus imply that the region of D-type asteroid formation was characterized by a significant D-enrichment relative to that of C-type asteroids (the only exception being CR chondrites, peculiar chondrites proposed to have formed in the outer part of the disk; van Kooten et al. 2016). The D enrichments of D-type asteroids are likely inherited from D-rich molecular cloud materials (i.e., organic and water–ice grains) that were not reprocessed by high-temperature thermal events, consistent with the low abundance of chondrules in Tarda and Tagish Lake. This conclusion is consistent with the occurrence in Tagish Lake of organic globules similar to those observed in cometary particles whose isotopic compositions are interpreted as being inherited from the cold molecular cloud from which the solar system formed (Nakamura-Messenger et al. 2006).

5. Conclusions

Our petrographic and isotopic surveys of the Tarda carbonaceous chondrite revealed that it shares important similarities with the Tagish Lake chondrite. Both likely originate from D-type asteroids, which are considered to have formed at large heliocentric distances beyond the current orbit of Saturn. By comparing our isotopic data with those from chondrites related to C-type asteroids, we showed that the outer solar system at the time of chondrite formation was characterized by large-scale O isotopic homogeneities in (i) the gas that drove the formation of FeO-poor chondrules and (ii) the water–ice grains accreted by carbonaceous asteroids. It also appears that the formation region of D-type asteroids is significantly enriched in deuterium relative to that of C-type asteroids due to the accretion of unprocessed, D-rich materials from the molecular cloud.

6. Research Data

Original data from this study are available on the Ordar database; [10.24396/ORDAR-63](https://doi.org/10.24396/ORDAR-63).

We thank Thomas Rigaudier, Johan Villeneuve, Dorian Thomassin, Pierrick Durand, and the Service d’Analyses des Roches et des Minéraux (SARM) for assistance with analyses. We thank Wataru Fujiya for constructive comments and Associate Editor Maria Womack for careful editing. This is CRPG contribution #2770.

Appendix Material and Method

A.1. Mineralogical and Petrographic Observations

We surveyed two homemade thick sections of Tarda (Tarda #1 and #2) in reflected light. Scanning electron microscope (SEM) observations and Energy Dispersive X-ray (EDX) spectral analyses were performed at CRPG with a JEOL JSM-6510 equipped with an EDX Genesis X-ray detector and operating with a 3 nA primary beam at 15 kV. Quantitative analyses of the mineralogical compositions of chondrule olivine grains were made with a CAMECA SX-100 electron microprobe (SCMEM) at the University of Lorraine. A 20 nA focused beam, accelerated to 15 kV potential difference, was used for spot analyses of silicates. Detection limits in silicates

were (i) 0.03 wt% for SiO₂, Al₂O₃, CaO, and MgO, (ii) 0.04 wt% for MnO and TiO₂, and (iii) 0.07 wt% for NiO, Cr₂O₃, and FeO.

A.2. X-Ray Diffraction

500 mg of Tarda were gently crushed in an agate mortar for determining its XRD patterns. The measurements were performed using a Panalytical X’Pert Pro diffractometer equipped with a Cu tube, a Ge(111) incident-beam monochromator ($K\alpha_1 = 1.5406 \text{ \AA}$), 0.02 rad Soller slits, programmable divergence and antiscatter slits, the irradiated area was fixed to 10 mm × 10 mm and an X’Celerator fast detector. The X’Celerator detector was used as “scanning line detector (1D)” with 2°122 active length. Phase identification was realized using the Panalytical software “X’Pert Highscore Plus” with the pdf2 files as crystallographic database.

A.3. Bulk Chemistry

Two fragments were prepared and the results are listed in Table 3. Both samples were crushed into powder in an agate mortar. The second sample (Tarda 2) corresponds to the fraction that was used for determining the XRD pattern. Trace element concentrations were measured with a Thermo® ICP-MS iCapQ (Tarda 1, CRPG) and a Thermo® Element2 HR-ICP-MS at CRPG (Tarda 2, IUEM). 120 mg of powder was digested on a hot plate heated to 125°C, using sequential mixtures of HF/HNO₃, HNO₃, and HCl. Concentrations were determined following the procedure described by Barrat et al. (2012, 2016). The reproducibility is always much better than 5%.

A.4. Bulk Hydrogen, Carbon, and Nitrogen Isotope Measurements

The hydrogen, carbon, and nitrogen concentration and isotopic composition of Tarda has been determined using a Thermo Scientific EA IsoLink—DeltaV IRMS System at CRPG. The procedure was similar to that detailed in Vacher et al. (2020). After crushing in an agate mortar, two aliquots (3.36 and 4.29 mg, respectively) were loaded into tin capsules, which were degassed for 48 hr at 120°C for removing adsorbed atmospheric water before hydrogen measurements (Vacher et al. 2016; Marrocchi et al. 2020; Piani et al. 2020). We express the hydrogen isotopic compositions in delta units relative to that of Standard Mean Ocean Water (SMOW, $D/H_{SMOW} = 155.76 \times 10^{-6}$) with $\delta D[\text{‰}] = [(D/H_{\text{sample}}/D/H_{SMOW}) - 1] \times 1,000$. Reproducibilities estimated from reference materials are better than 10% (2σ) for H concentration and 5‰ for δD . Aliquots of 5–10 mg were wrapped in tin foil and used for C and N measurements. The capsule was loaded into an auto-sampler connected to the EA system and pumped for 20 minutes before oxidation on a reactor made of a quartz tube filled with Cr₂O₃. The tin capsule oxidation led to exothermic reactions (up to 180°C) releasing N₂ and CO₂ which were separated on a chromatographic column at 70°C. For nitrogen analyses, 2σ errors are expected to be 10% for [N] and 2‰ for $\delta^{15}\text{N}$. Errors on [C] are estimated to be 2% and 2‰ for $\delta^{13}\text{C}$.

A.5. In Situ Oxygen Isotopic Compositions

Olivine oxygen isotopic compositions of chondrule olivine grains were determined at CRPG using a CAMECA IMS 1270

E7. $^{16}\text{O}^-$, $^{17}\text{O}^-$, and $^{18}\text{O}^-$ ions produced by a Cs^+ primary beam of 500 pA ($\sim 4 \mu\text{m}$) were measured in multicollection mode using two off-axis Faraday cups and the axial electron multiplier (EM). A normal-incidence electron gun was used for charge self-compensation. To remove interference from $^{16}\text{OH}^-$ on the $^{17}\text{O}^-$ peak and maximize the flatness atop the $^{16}\text{O}^-$ and $^{18}\text{O}^-$ peaks, the entrance ($\sim 100 \mu\text{m}$), and axial exit ($\sim 200 \mu\text{m}$) slits were adjusted to obtain a mass resolving power ($\text{MRP} = M/\Delta M$) of ~ 6000 for $^{17}\text{O}^-$ on the axial EM. $^{16}\text{O}^-$ and $^{18}\text{O}^-$ were measured on L'2 and H1 (slit 1, $\text{MRP} \approx 2500$; Bouden et al. 2021). For removing the carbon coating at the surface, samples were sputtered before each measurement for 90 s over an area of $2 \times 2 \mu\text{m}$. 40 cycles of 5 s each were acquired to obtain counting statistics on the order of $\pm 0.6\%$ (2σ) for $\delta^{18}\text{O}$ and 0.4% (2σ) $\delta^{17}\text{O}$. Three terrestrial standards were measured to define the mass fractionation line (Diopside, magnetite, and San Carlos olivine) and to correct instrumental fractionation due to the matrix effect of olivine. Typical measurement errors of $\sim 0.4\%$ – 0.7% for $\delta^{18}\text{O}$, $\delta^{17}\text{O}$, and $\Delta^{17}\text{O}$ (2σ) account for internal errors on each measurement and the external reproducibility of the standard.

ORCID iDs

Yves Marrocchi  <https://orcid.org/0000-0001-7075-3698>
Guillaume Avice  <https://orcid.org/0000-0003-0962-0049>

References

- Alexander, C. M. O., Bowden, R., Fogel, M. L., et al. 2012, *Sci*, **337**, 721
 Baker, L., Franchi, I. A., Wright, I. P., & Pillinger, C. T. 2002, *M&PS*, **37**, 977
 Barrat, J.-A., Dauphas, N., Gillet, P., et al. 2016, *GeCoA*, **176**, 1
 Barrat, J.-A., Zanda, B., Moynier, F., et al. 2012, *GeCoA*, **83**, 79
 Barucci, M. A., Perna, D., Popescu, M., et al. 2018, *MNRAS*, **476**, 4481
 Bouden, N., Villeneuve, J., Marrocchi, Y., et al. 2021, *FrEaS*, **8**, 9
 Brown, P. G., Hildebrand, A. R., Zolensky, M. E., et al. 2000, *Sci*, **290**, 320
 Byrson, J. M. J., Weiss, B. P., Biersteker, J. B., et al. 2020, *ApJ*, **896**, 103
 Chennaoui Aoudjehane, H., Agee, C. B., Ziegler, K., et al. 2021, *LPI*, **52**, 1928
 Clayton, R. N., & Mayeda, T. K. 1984, *EPSL*, **67**, 151
 Delbo, M., Walsh, K., Bolin, B., Avdellidou, C., & Morbidelli, A. 2017, *Sci*, **357**, 1026
 DeMeo, F. E., & Carry, B. 2014, *Natur*, **505**, 629
 Dey, S., Yin, Q.-Z., & Zolensky, M. 2021, *LPI*, **52**, 2517
 Doyle, P. M., Jogo, K., Nagashima, K., et al. 2015, *NatCo*, **6**, 7444
 Friedrich, J. M., Wang, M.-S., & Lipschutz, M. E. 2002, *M&PS*, **37**, 677
 Fujiya, W., Hoppe, P., Ushikubo, T., et al. 2019, *NatAs*, **3**, 910
 Gartelle, G. M., Hardersen, P. S., Izawa, M. R. M., & Nowinski, M. C. 2021, *Icar*, **354**, 114043
 Hiroi, T., Tonui, E., Pieters, C. M., et al. 2005, *LPI*, **36**, 1564
 Hiroi, T., Zolensky, M. E., & Pieters, C. M. 2001, *Sci*, **293**, 2234
 Izawa, M. R. M., Craig, M. A., Applin, D. M., et al. 2015, *Icar*, **254**, 324
 Jacquet, E., Piralla, M., Kersaho, P., et al. 2021, *M&PS*, **56**, 13
 King, A. J., Bates, H. C., Krietsch, D., et al. 2019, *Geoch*, **79**, 125531
 King, A. J., Bates, H. C., Schofield, P. F., & Russell, S. S. 2021, *LPI*, **52**, 1909
 Krot, A. N., Nagashima, K., Lyons, J. R., Lee, J.-E., & Bizzarro, M. 2020, *SciA*, **6**, eaay2724
 Le Guillou, C., Changela, H. G., & Brearley, A. J. 2015, *EPSL*, **420**, 162
 Levison, H. F., Bottke, W. F., Gounelle, M., & Morbidelli, A. 2009, *Natur*, **460**, 364
 Marrocchi, Y., Bonal, L., Gattacceca, J., et al. 2020, *M&PS*, **55**, 1924
 Marrocchi, Y., Euverte, R., Villeneuve, J., et al. 2019, *GeCoA*, **247**, 121
 Marrocchi, Y., Villeneuve, J., Batanova, V., Piani, L., & Jacquet, E. 2018, *EPSL*, **496**, 132
 Morbidelli, A., Levison, H. F., Tsiganis, K., & Gomes, R. 2005, *Natur*, **435**, 462
 Nakamura, T., Noguchi, T., Kimura, Y., et al. 2013, *M&PSA*, **76**, 5122
 Nakamura-Messenger, K., Messenger, S., Keller, L. P., Clemett, S. J., & Zolensky, M. E. 2006, *Sci*, **314**, 1439
 Oglione, R., Huss, G. R., Hagoashima, K., et al. 2012, *ApJL*, **745**, L19
 Patzek, M., Hoppe, P., Bischoff, A., Visser, R., & John, T. 2020, *GeCoA*, **272**, 177
 Piani, L., Marrocchi, Y., Rigaudier, T., et al. 2020, *Sci*, **369**, 1110
 Piralla, M., Marrocchi, Y., Verdier-Paoletti, M. J., et al. 2020, *GeCoA*, **269**, 451
 Pourmand, A., Dauphas, N., & Ireland, T. J. 2012, *ChGeo*, **291**, 38
 Sugiura, N., & Fujiya, W. 2014, *M&PS*, **49**, 772
 Sutton, S., Alexander, C. M. O., Bryant, A., et al. 2017, *GeCoA*, **211**, 115
 Tenner, T. J., Ushikubo, T., Nakashima, D., et al. 2018, in *Chondrules: Records of Protoplanetary Disk Processes*, ed. S. S. Russell, H. C. Connolly, Jr., & A. N. Krot (Cambridge: Cambridge Univ. Press), 196
 Ushikubo, T., & Kimura, M. 2021, *GeCoA*, **293**, 328
 Ushikubo, T., Kimura, M., Kita, N. T., et al. 2012, *GeCoA*, **90**, 242
 Vacher, L. G., Marrocchi, Y., Verdier-Paoletti, M. J., et al. 2016, *ApJL*, **827**, L1
 Vacher, L. G., Orgliore, R. C., & Liu, N. 2021, *LPI*, **52**, 2528
 Vacher, L. G., Piani, L., Rigaudier, T., et al. 2020, *GeCoA*, **281**, 53
 van Kooten, E. M. M. E., Wielandt, D., Schiller, M., et al. 2016, *PNAS*, **113**, 2011
 Vernazza, P., Castillo-Rogez, J., Beck, P., et al. 2017, *AJ*, **153**, 72
 Vokrouhlický, D., Bottke, W. F., & Nesvorný, D. 2016, *AJ*, **152**, 39
 Weiss, B. P., Bai, X.-N., & Fu, R. R. 2021, *SciA*, **7**, eaba5967
 Yamamoto, D., Kuroda, M., Tachibana, S., Sakamoto, N., & Yurimoto, H. 2018, *ApJ*, **865**, 98